Geomechanics and Engineering, *Vol. 16, No. 1 (2018) 49-58*
DOI: https://doi.org/10.12989/gae.2018.16.1.049

Crack behaviour of top layer in layered rocks

Xu Chang[1,2], Wenya Ma[2], Zhenhua Li[*2] and Hui Wang[2]

[1]*International Joint Research Laboratory of Henan Province for Underground Space Development and Disaster Prevention, Jiaozuo, China*
[2]*School of Civil Engineering, Henan Polytechnic University, Jiaozuo, China*

(Received June 29, 2017, Revised March 11, 2018, Accepted March 15, 2018)

Abstract. Open-mode cracks could be commonly observed in layered rocks. A concept model is firstly used to explore the mechanism of the vertical cracks (VCs) in the top layer. Then the crack behaviour of the two-layer model is simulated based on a cohesive zone model (CZM) for layer interfaces and a plastic-damage model for rocks. The model indicates that the tensile stress normal to the VCs changes to compression if the crack spacing to layer thickness ratio is lower than a threshold. The results indicate that there is a threshold for interfacial shear strength that controls the crack patterns of the layered system. If the shear strength is lower than the threshold, the top layer is meshed by the VCs and interfacial cracks (ICs). When the shear strength is higher than the threshold, the top layer is meshed by the VCs and parallel cracks (PCs). If the shear strength is comparative to the threshold, a combining pattern of VCs, PCs and ICs for the top layer can be formed. The evolutions of stress distribution in the crack-bound block indicate that the ICs and PCs can reduce the load transferred for the substrate layer, and thus leads to a crack saturation state.

Keywords: interface cracks; vertical crack; parallel crack; shear strength; layered rock

1. Introduction

Opening-mode cracks are extremely common in the layered rocks (Liu *et al* 2017, Ferrill *et al.* 2012, Chang *et al*. 2015, Arora and Mishra, 2015, Jesus *et al*. 2016). Many field observations, physical experiments and numerical models have revealed that there is a direct connection between the crack spacing and the thickness of cracked layers. In situ studies by Bejari and Hamidi (2013), Gross *et al*. (1995), Guo *et al*. (2017) indicated crack spacing in the rock sequences was approximatively proportional to the cracked layer thickness. The crack formation process was described as 'crack infilling' and final state that no new cracks can further infill was the 'crack saturation'. Tang *et al*. (2008) demonstrated crack infilling process based on a progressive damaged model. Their study indicated that the stress sate in a crack-bound block also changed from tensile to compressive if the crack spacing decreased to a low level.

These aforementioned experimental, analytical and numerical analyses, including revealing the relationship between the cracked layer thickness and the crack spacing or the mechanical explanation for crack saturation, are mostly based on the three-layer model. For a layered-rock system, there always exists a top layer, as indicated in Fig.1, which is quite different from other layers because it has only one bounding layer, the substrate one. This indicates that the crack behaviour for the top layer should be different from other layers; however, the crack behaviour of the top rock layer is seldom considered. Engelder and Fischer (1996) have systematically investigated driving mechanisms for cracks in rock based on Griffith energy-balance concept, including mud cracks and columnar jointing and their studies greatly improve the understanding of cracks in rocks. However, the formation mechanisms for those parallel discontinuities and their interaction with those VCs in layered rock are still unclear. The lack of investigation of the crack behaviour of the top layer has limited the deep and complete understanding of the crack spacing problem of layered rocks. Obviously, the extensively adopted three-layer model is not suitable for further investigation of crack behaviour of the top layer. In this study, a two-layer model is therefore developed to investigate the crack behaviour of the top layer of the rock sequences. The interface is defined as the bound between layers.

Fig. 1 Examples of crack pattern for top rock layer. The vertical cracks are periodically distributed

∗Corresponding author, Professor
E-mail: jzlizhenh@163.com

ISSN: 2005-307X (Print), 2092-6219 (Online)

2. Numerical model

Continuum damage mechanics has become a common tool to solve the multi-cracking problem. In this study, also, a plastic damage model is adopted to simulate the progressive failure of rocks. The Drucker-Prager yield criterion is adopted (Ben-Zion and Lyakhovsky 2002), which is described as

$$\alpha I + \sqrt{J_2} = k \tag{1}$$

$$J_2 = [(\sigma_1 - \sigma_2)^2 + (\sigma_2 - \sigma_3)^2 + (\sigma_3 - \sigma_1)^2]/6 \tag{2}$$

$$I = \sigma_1 + \sigma_2 + \sigma_3 \tag{3}$$

where σ_1, σ_2 and σ_3 are the three principal stress.

$$\alpha = \frac{\sin\varphi}{\sqrt{3(3+\sin^2\varphi)}} \tag{4}$$

$$k = \frac{\sqrt{3}c\cos\varphi}{\sqrt{3+\sin^2\varphi}} \tag{5}$$

where c and φ is the cohesion and angle of internal friction.

The yield function can be described as (ABAQUS, 2009)

$$F(\sigma^{ef}, \varepsilon^{pl}) = \frac{1}{1-\zeta}(q - 3p\zeta + \beta(\varepsilon^{pl})\langle\sigma^{ef}_{\max}\rangle) - \frac{1}{1-\zeta}\gamma\langle\sigma^{ef}_{\max}\rangle - \sigma_c^{ef}(\varepsilon_c^{pl}) \le 0 \tag{6}$$

with

$$\zeta = \frac{\sigma_{b0} - \sigma_{c0}}{2\sigma_{b0} - \sigma_{c0}} \quad 0 \le \zeta < 0.5 \tag{7}$$

$$\gamma = \frac{3(1-K_c)}{2K_c - 1} \tag{8}$$

where ε_c^{pl} is effective plastic strain for compression) and ε_t^{pl} is effective plastic strain for tension; ζ and γ are the material constant; σ_{b0}/σ_{c0} is the initial equibiaxial compressive yield stress to initial unaxial compressive yield stress ratio; $\sigma^{ef}_{\max}$ is the maximum principal effective stress. K_c is the shape of yield function in meridian plane. q and p are the Mises equivalent stress and the hydrostatic pressure, respectively.

The stress-strain relations for the material under compressive as well as tensile loading is need to reflect the material response. A damage variable (d) is employed to account for the progressive degradation of the material. For the rock material under compression, the stress-strain relationship proposed by Aydan *et al.* (1993) is adopted (indicated in Fig. 2(a))

$$\varepsilon_c^{pl} = 2\sigma_c^{-0.17} \cdot \varepsilon_e \tag{10}$$

where ε_e is the maximum elastic strain; ε_c^{pl} is the plastic strain and σ_c is the compressive strength in MPa.

For rock mass under compression, the evolution of the compressive damage (d_c) can be determined by the Eq. (11) (Tang 1997)

$$d_c = \begin{cases} 0 & \varepsilon_c < \varepsilon_c^0 \\ 1 - \dfrac{\sigma_c}{E_c\varepsilon_c} & \varepsilon_c^0 < \varepsilon_c < \varepsilon_{c\lim} \\ 1 & \varepsilon_{c\lim} < \varepsilon_c \end{cases} \tag{11}$$

where ε_c^0 is the compressive strain at peak stress; and $\varepsilon_{c\lim}$ is the ultimate strain at failure.

And the tensile damage variable(d_t)is described as (Tang 1997)

$$d_t = \begin{cases} 0 & \varepsilon_t < \varepsilon_t^0 \\ 1 - \dfrac{\sigma_t}{E_c\varepsilon_t} & \varepsilon_t^0 < \varepsilon_t < \varepsilon_{t\lim} \\ 1 & \varepsilon_{t\lim} < \varepsilon_t \end{cases} \tag{12}$$

where ε_t^0 is the tensile strain at elastic limit; and $\varepsilon_{t\lim}$ is the ultimate strain at failure. And E_c is the elastic modulus for the rock mass. Examples for evolution of these damage variables are illustrated in Fig. 2.

The common approach for interaction between layers is too simplified that the layers are bonded together without any slip. The Coulomb friction model (indicated in Fig. 2(e)) relates the shear stress across the interface to the contact pressure between the rock layers. The Coulomb friction model cannot capture the stress decrement along the interface. In recent years, the cohesive zone model (CZM) suggested by Dugdale (1960) has been extensively adopted to describe the interaction between two materials, due to its simple formulation (Shor and Vaziri, 2017 and Zhang 2017). In this paper, as an attempt to model the interfacial behaviour, the CZM is introduced to model interfaces between layers. The properties of the CZM are defined by a traction model (Fig. 2(f)). The shear stress (τ) is mobilized by and proportional to the relative shear displacement (δ). As the ascending branch increases to the shear strength ($\tau_{\max}$), a linear softening branch followed and then a constant stage. The relationship between the shear strength and the residual shear strength (τ_r) can be described as

$$\tau_r = \beta\tau_{\max} \tag{13}$$

where β is residual shear strength factor.

As stated before, a two-layer model composted of top layer and its substrate layer is developed in this study. The FEM model is indicated in Fig. 3. The four-node plane element (CPS4R) is used for the rock layers. And the cohesive element (COH2D4) is adopted for the cohesive

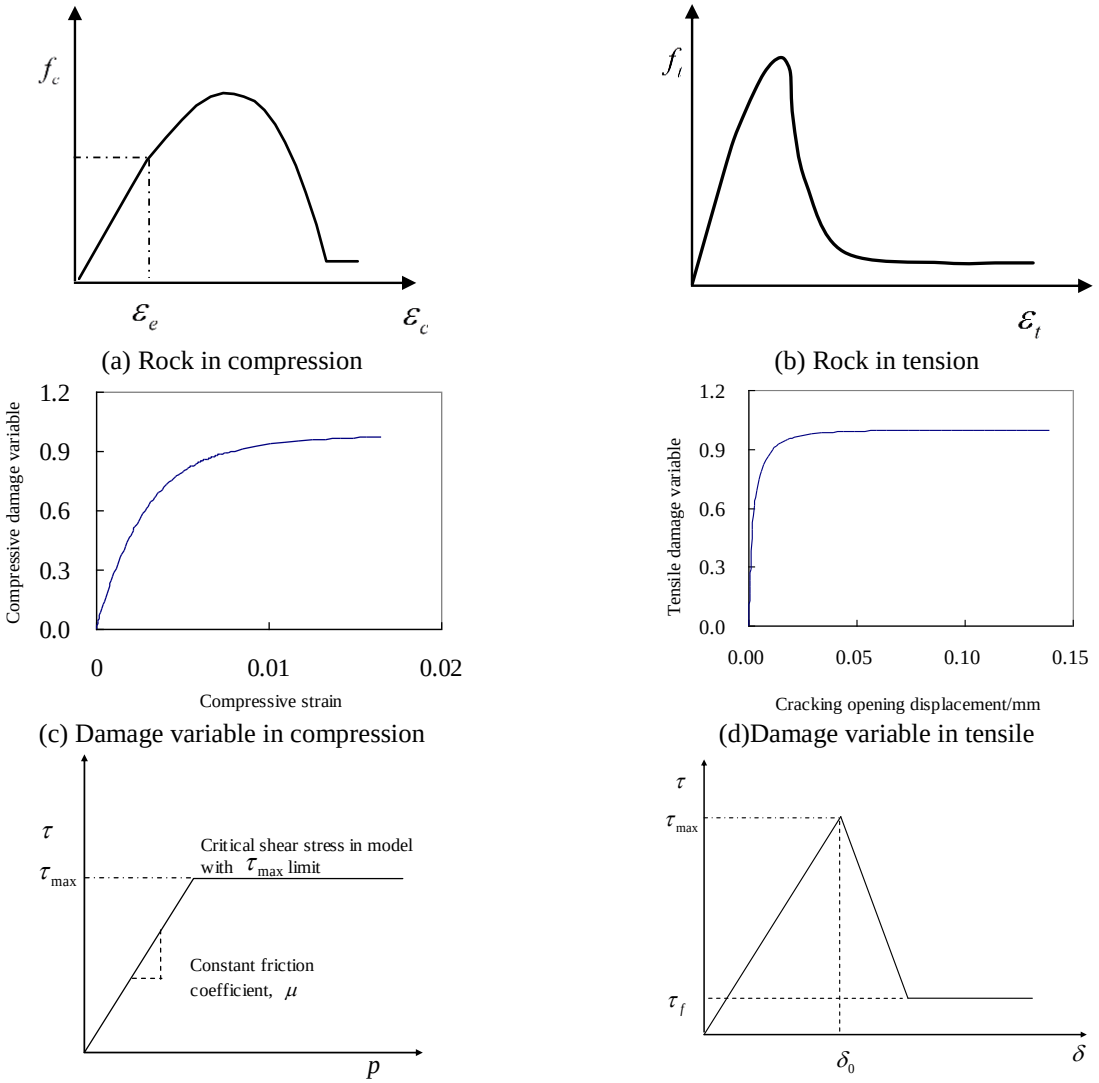

(a) Rock in compression (b) Rock in tension

(c) Damage variable in compression (d)Damage variable in tensile

(e) Column model (f) CZM model

Fig. 2 Material models: f_c and ε_c are compressive stress and strain for rock under compressive; f_t and ε_t are tensile stress and strain for rock under tensile condition

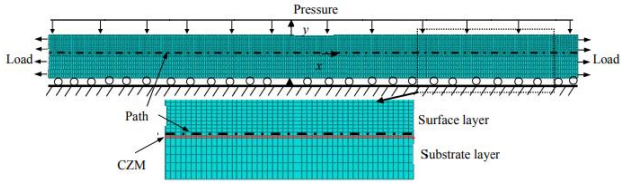

Fig. 3 Element mesh and boundary conditions for two-layer rock system. *x* direction is parallel to the layers and *y* direction is vertical to the layers. The CZM is a very thin layer between the top layer and its substrate layer. A path is defined along the bottom boundary of the top layer

zone. In this study, the Young modulus, Poisson's ratio and compressive strength for the top layer are 50GPa, 0.2 and100MPa, respectively. And the Young modulus, Poisson's ratio and compressive strength for the top layer are 15GPa, 0.2 and 300 MPa, respectively (Li *et al*. 2012).

The thickness for the top layer is 20mm. The substrate layer has the same thickness of 20 mm. The model has a width of 500 mm. For this layered model, the top layer and its substrate layer are connected by the CZM. The bottom of the model in the direction (vertical to the layers) is fixed and its middle in the direction (parallel to the layers) is also fixed. Displacements are applied on the right and left sides. The existing studies indicated that these cracks in the layered rock may form at depth and carry to the surface during exhumation (Engelder *et al.* 2009). Therefore, a constant overburden pressure (P) is applied at the top boundary.

3. Numerical results

3.1 Model verification

As mentioned above, crack spacing by three-layer system have been extensively investigated and the results are well accepted. Therefore, the three-layer system is firstly used to verify the model adopted in this paper. In the

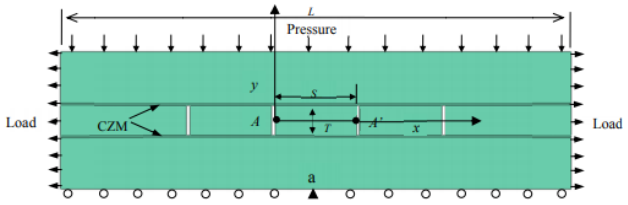

(a) Model for layered rocks with four equally spacing cracks. The *x*-axis is parallel to the interfaces and perpendicular to the cracks. The *y*-axis is perpendicular to the layer interfaces. The bottom boundary is fixed in *y*-direction, with the middle point fixed in the *x*-direction as well. A displacement is imposed on the left and right sides of the model and a pressure is applied on the top

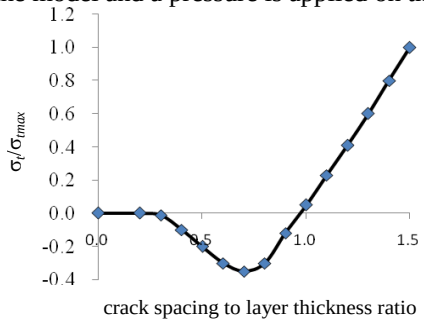

(b) Results of Bai and Pollard (2000)

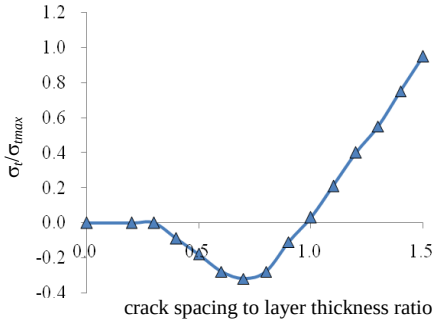

(c) Results from this study

Fig. 4 Verification of the numerical model

same method (Bai *et al.* 2000, Tang *et al.* 2008), a three-layer system with four cracks pre-assigned in the central layer is adopted, as indicated in Fig 4(a). These four cracks are equally spaced and vertical to the layer interfaces. The central layer thickness is T_f=20 mm. The model thickness is 80 mm. The model bottom is fixed in the y-direction and it's the middle point is further fixed in the *x*-direction. Uniform tensile loads are applied at the left and right boundaries in *x*-direction. Following Bai *et al.* (2000), the three-layer system is loaded by a constant pressure of 5 MPa in *y*-direction. The materials parameters are also same as those used by Bai *et al.* (2000) and Tang *et al.* (2008). Then the evolution of the stress distribution is examined with various crack spacing to the cracked layer thickness ratios. In their studies, the layer interfaces are assumed to be perfectly welded; therefore, an enough high shear strength (18 MPa) for interface is adopted to preclude the interface cracks.

As shown in Fig. 4(b) and 4(c), the normalized stress (σ_x/σ_{xmax}) at the midpoint varies with different crack spacing to the cracked layer thickness ratios. It indicates that the

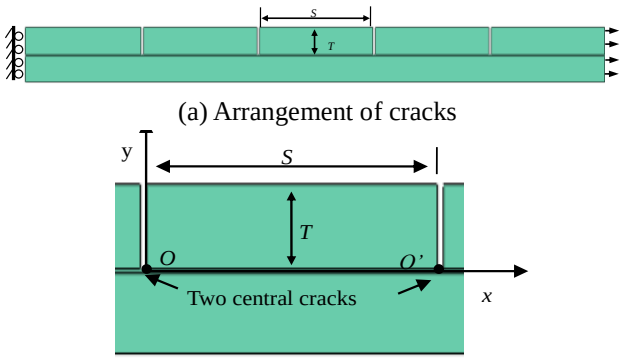

(a) Arrangement of cracks

(b) Details for two central cracks. *T* is the thickness of the crack layer and *S* is the crack spacing. Line *OO*' is between the two central cracks along the bottom boundary of the surface layer

Fig. 5 Numerical model for two-layer system with four pre-assigned vertical cracks

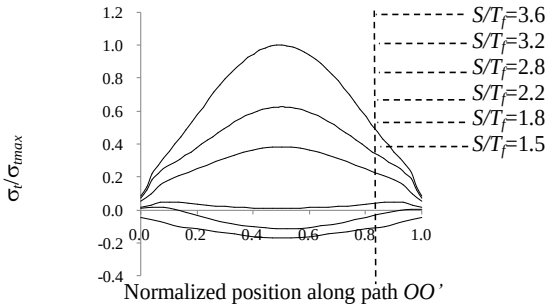

Fig. 6 Stress state between two central cracks changes from tensile to compressive with the decreasing of crack spacing to layer thickness ratio (*S*/*T*). The tensile stress is positive while the compressive stress is negative

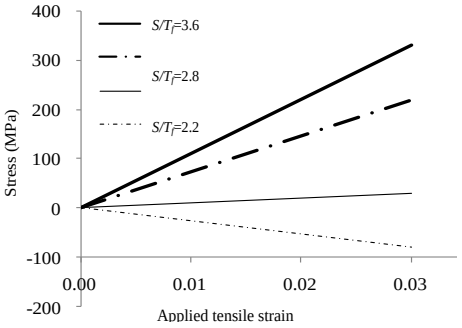

Fig. 7 Normal stress in the direction perpendicular to cracks at middle point of *OO'* as a function of applied tensile strain for various crack spacing to layer thickness ratios (*S*/*T*). The tensile stress is positive while the compressive stress is negative

threshold for crack spacing to the cracked layer thickness ratio is about 1.0. This threshold determines the stress state between the adjacent cracks: when the crack spacing to the cracked layer thickness ratio is lower this threshold the normal stress along the line AA' is compressive, and if the crack spacing to the cracked layer thickness ratio is greater than the threshold the normal stress is tensile. The results agree well with the results obtained by Bai *et al.* (2000).

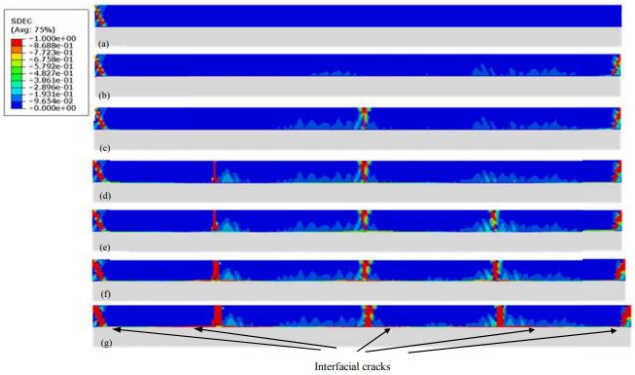

Fig. 8 Crack process for interface shear strength of 7.2 MPa. SDEG ranging from zero to one is used to describe the evolution of damage variable

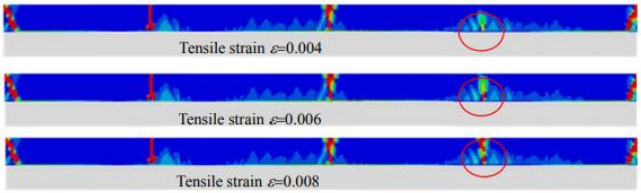

Fig. 9 A typical evolution process of the VC. The VC always initiates at the bottom of the top layer and propagates to its top. SDEG ranging from zero to one is used to describe the evolution of damage variable

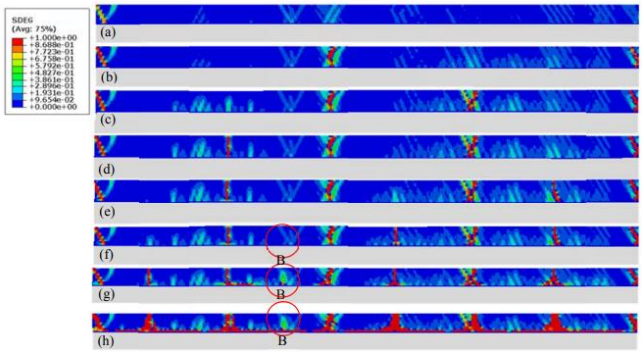

Fig. 10 Crack process for the interface shear strength of 16.0 MPa. A VC initiates at point B; however, it cannot further propagate to the top of the top layer due to the occurrence of the PCs

3.2 Evolution of stress state

To clear understanding the formation mechanisms of the VCs in the top layer, the stress distribution that governs the crack behaviour is also investigated firstly and the failure for the two-layer system are not considered in this section. A conceptual model with four VCs existing in the top layer is also adopted. These cracks have the equal spacing with an opening of 2 mm, as indicated in Fig. 5. Also, a constant overburden pressure of 2 MPa is applied on the top of the model.

With this three-layer system, the evolution of the stress state is investigated with varied crack spacing (S) to cracked layer thickness (T_f) ratio (S/T_f). To show how the stress distribution varies as a function of S/T_f, the distribution of

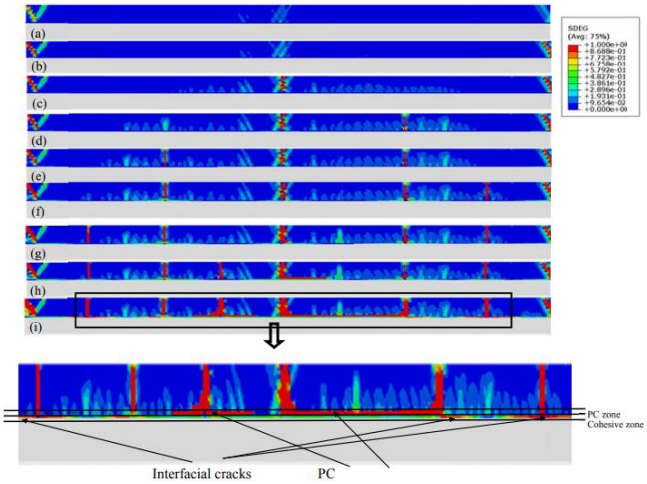

Fig. 11 Crack process for the interface shear strength of 12 MPa. The PCs propagate in a thin layer of the top layer near the bottom boundary while the interfacial cracks propagates in the cohesive zone

normalized normal stress (σ_x/σ_{xmax}) versus the normalized position (x/S) along line OO' for various S/T_f is shown in Fig. 5, where the tensile stress is positive. The two-layer model is elastic and the failure for the rock and interface is not considered in this section. For all the models, the elastic constants are same and the applied tensile strain is also the same of 0.01. According to Fig. 6, the stress is tensile when S/T_f is 2.2 or greater; while the stress along the line OO' changes to compression (negative) if the ratio is less than 2.2. This indicates that there exists a threshold for S/T_f, which characterizes the stress state transition between the two cracks. This conclusion is similar to Bai *et al.* (2000) from the three-layer model except that the threshold for S/T_f is about 1.0 even with the same material parameters. Fig. 7 gives the values of σ_x at middle point of line OO' for different applied tensile strain. It can be seen that the applied tensile strain only affects the magnitude of the tensile stress but not its sign. Therefore, the threshold for S/T_f is independent of the applied tensile load.

3.3 Crack patterns

It can be confirmed there exists a stress state transition in a crack-bound block in the two-layer system based on discussion in previous section. In this section the crack behaviour of the two-layer system but without existing cracks is modeled.

Fig. 8 shows the numerical crack infilling process for the interface shear strength is 7.2 MPa. Firstly (Figs. 8(a)-8(e)), the VCs initiate at the bottom of the top layer and propagates to its top. A typical evolution process of VC is indicated in Fig. 9. With the increasing of tensile load, the new VCs sequentially infill between two adjacent early formed cracks. In the second stage (Figs. 8(f)-8(k)), the ICs occurs near these VCs as the applied tensile load reaches a certain value. In the following stage, the ICs initiates at the ends of the VCs and propagates to their adjacent cracks. The ICs can decrease the stress transferred from the substrate layer, and thus no more new cracks can further

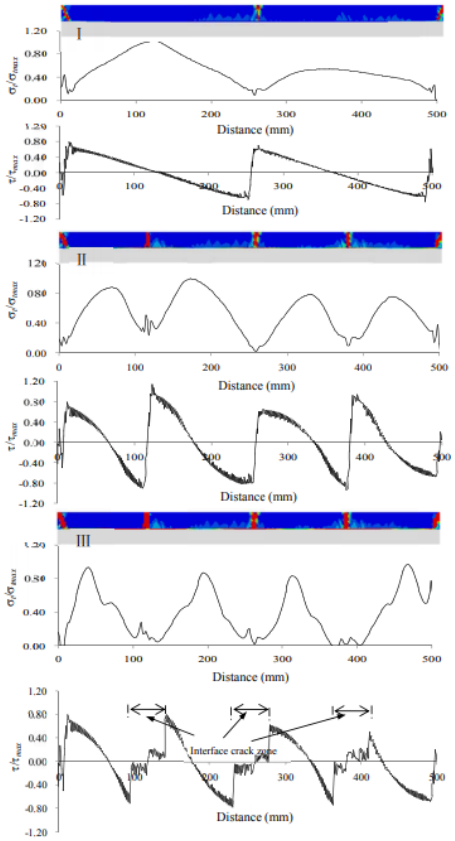

Fig. 12 Evolution of tensile stress along the path and interfacial shear stress for case of shear strength higher than the threshold (τ_{max}=7.2 MPa, τ_{cr}=12 MPa). The letter 'P' indicates the parallel crack zone

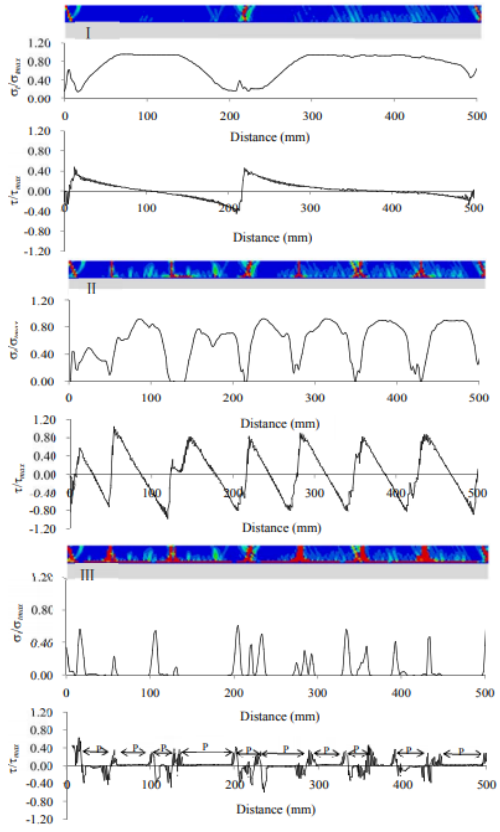

Fig. 13 Evolution of tensile stress along the path and interfacial shear stress for case of shear strength higher than the threshold (τ_{max}=16 MPa, τ_{cr}=12 MPa). The letter 'P' indicates the parallel crack zone

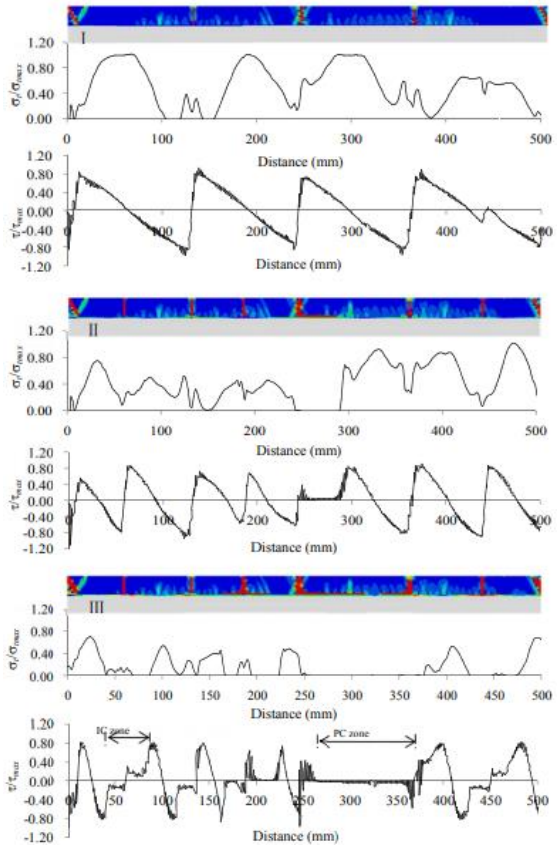

Fig. 14 Evolution of tensile stress along the path and interfacial shear stress for case of shear strength higher than the threshold (τ_{max}=12 MPa, τ_{cr}=12 MPa). The letter 'P' indicates the parallel crack zone

infill during the process of ICs. As a result, the state of "crack saturation" is obtained (Fig. 8(k)).

Fig. 10 shows the numerically obtained crack infilling process for the interface shear strength is 16.0 MPa. For this case, the crack process also consists of two stages. Firstly, the VCs are the dominated failures that the VCs infill continually between two earlier formed adjacent cracks (Figs. 10(a)-10(f)). Because of the high shear strength, no ICs can occur in this case. However, cracks parallel to the layer interface (parallel crack hereafter, PC)) can initiate at the ends of the VCs and propagate to their adjacent VCs in the second stage (Figs. 10(j)-(h)). Once the PC occurs, no more VCs can further infill. As indicated in Fig. 10, a VC initiates at point B, but it cannot propagate further to top of the top layer during propagation of the PCs. This indicates that the PCs can also decrease the stress transferred from the substrate layer to exclude the further infilling of the VCs.

Fig. 11 illustrates the crack process with interfacial shear strength of 12 MPa. For this case, the VCs initiate at the bottom of the top layer and propagate to its top is the first stage, which is the similar process of crack infilling. However, with the increasing of the applied tensile load, both the ICs and the PCs can be formed, as indicated in Figs 11h-j. It should be noted that both the ICs and the PCs are parallel to the layer interfaces; however, they are quite different. The ICs occur in the cohesive zone between two layers; while the PCs mainly form in a thin zone near the interface, as illustrated in Fig. 11(i).

Figs. 8, 10 and 11 give three typical crack processes for cases with different interfacial shear strength. Further analysis indicates that if the interfacial shear strength is lower than 12 MPa, only the ICs occurs after crack infilling process. If the interface shear strength is greater than 12 MPa, the PCs are formed while the ICs is excluded. Therefore, the crack pattern of the two-layer system seems to be controlled by the interfacial shear strength. There exists a threshold for interfacial shear strength (τ_{cr}): If τ_{max} is lower than τ_{cr}, the VCs in the top layer and ICs can occur; If τ_{max} is greater than τ_{cr}, the top layer is cracked by the VCs and PCs; If τ_{max} is comparative to τ_{cr}, a combining pattern of VCs, PCs and IC can be observed. For the given material parameters mentioned above, the threshold for shear strength of the two-layer system is about 12 MPa.

In the existing studies, the VCs in the layered rocks are extensively investigated; however, the discontinuities parallel to the layer is seldom discussed. According to the crack patterns of the layer system, the discontinuities parallel to the layers are induced by ICs, PCs, or their coupling behaviour.

3.4 Evolution of stress distributions during crack infilling process

To further explore the stress distributions during the crack infilling process, a path along the bottom line of the top layer is defined, as indicated in Fig. 3. The evolutions of the tensile stress along the path for these three typical crack

patterns are presented in Figs. 12, 13 and 14 as well as the interfacial shear stress, where tensile stress and interfacial shear stress are normalized by their maximum values.

The evolutions of the tensile stress and shear stress for case of $\tau_{max}<\tau_{cr}$ (τ_{max}=7.2 MPa, τ_{cr}=12 MPa) are illustrated in Fig. 12. For each crack-bound block, the tensile stress at the middle location along the path always reaches its peak value and therefore new crack is easy to initiate at this location. Once a VC forms, the tensile stress at the crack drops to zero. Because of the stress concentration near the VCs, the ICs always initiates at the ends of the VCs, as indicated in Fig.12. The ICs can obviously reduce the tensile stress in the crack-bound blocks and thus exclude the further infilling of the VC.

For case of $\tau_{max}>\tau_{cr}$ (τ_{max}=16.0 MPa, τ_{cr}=12 MPa), the evolutions of the tensile stress and shear stress are presented in Fig. 13. Before formation of the PCs, the distributions of the tensile stress and interfacial shear stress are similar to case of interfacial shear strength lower than the threshold. If the VCs form, the tensile load between two adjacent VCs in the top layer is transmitted from the substrate layer through the interfaces. It can be seen from Fig. 13 I and II the tensile stress near a VC is almost zero; however, the shear stress reaches its peak value near a VC. According to Fig 13 I and II, the peak shear stress always exists at the tip of a PC during its propagation process. This indicates that the interfacial shear stress induces the PCs. With the propagation of the PCs, the tensile stress for each crack-bound block and the interfacial shear stress drop to zero, as indicated in Fig. 13 III. Therefore, the formation of the PCs also reduces the load transmitted from the substrate layer and in turn to exclude the infilling of the VCs.

Fig. 14 shows the evolutions of tensile stress and shear stress for case of τ_{max} comparative to τ_{cr} (τ_{max} =12.0 MPa, τ_{max}=12 MPa) It is indicated that the PCs can reduce the tensile stress and shear stress to zero. However, residual tensile stress and interfacial shear stress exist for the cracks zone (Fig. 14III)

4. Parametric studies

4.1 Influence of shear strength of CZM on S/T_f

As discussed in this study, the crack spacing is kept constant after "crack saturation". Therefore, S/T_f at crack saturation (S_s/T_f) can be considered as an important parameter to reflect the behaviour of the layered system.

In this section, the shear strength τ_{max} with varied values is discussed. The relationship between S_s/T_f and τ_{max} is presented in Fig. 15. Once top layer is cracked by the tensile load no more VCs can further form since the tensile load cannot be transmitted from the adjacent layers with the shear strength of zero. Thus, the average fracturing spacing is $L/2$ (L is the length of the top layer) and S_s/T_f achieves it maximum value of 12.5 for case that shear strength is zero. The value of S_s/T_f decreases with increasing of the shear strength, as indicated in Fig. 15. However, S_s/T_f is almost kept the constant even with the further increasing of the shear strength if the shear strength is higher than 12 MPa. This means that the threshold for shear strength is 12

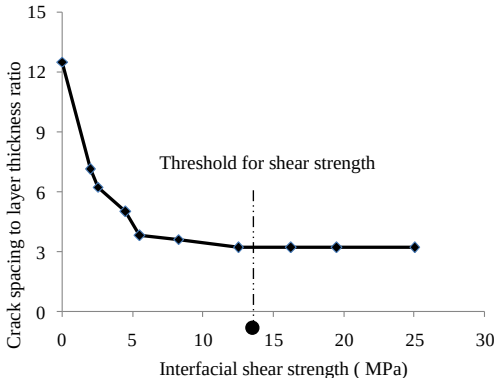

Fig. 15 Influence of shear strength on crack spacing to layer thickness ratio at crack saturation (S_s/T_f). If the interface shear strength (τ_{max}) is lower than 12 MPa, S_s/T_f decreases as increasing τ_{max}; If τ_{max} is greater than 12 MPa, S_s/T_f is kept constant with further increasing of τ_{max}. Thus, the point where S_s/T_f cannot further increase is defined as the threshold for interface shear strength (τ_{cr})

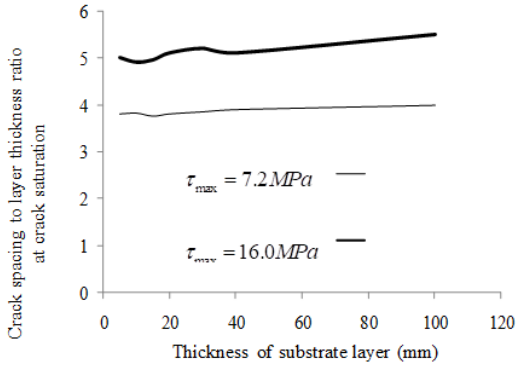

Fig. 16 Influences of thickness of substrate layer on crack spacing to layer thickness ratio at crack saturation (S_s/T_f)

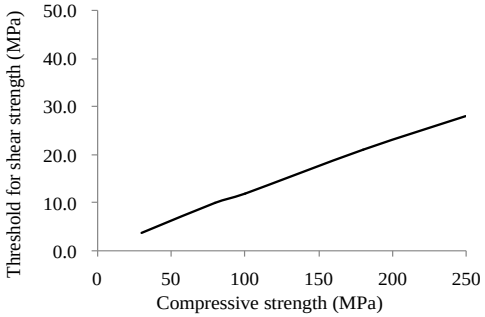

(a) Threshold for shear strength

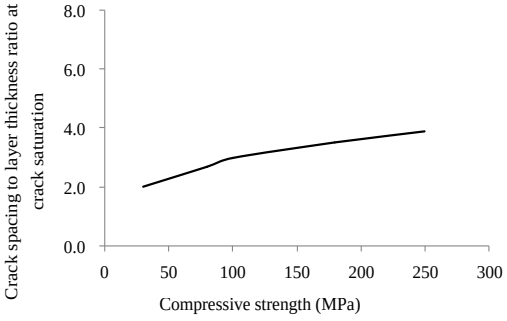

(b) Crack spacing to layer thickness ratio at crack saturation

Fig.17 Influences of compressive strength of top layer

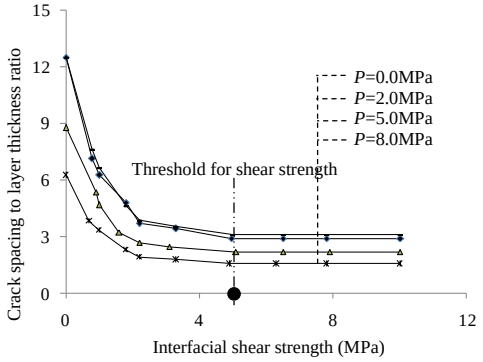

Fig. 18 Influences of overburden pressure

MPa. The corresponding S_s/T_f is about 3.2. Obviously, the shear strength has critical influences on S_s/T_f only for case of $\tau_{max} < \tau_{cr}$.

For the concept model mentioned above, S_s/T_f is about 1.3. However, S_s/T_f ranges from 12.5 to 3.2 if ICs and PCs are considered. This demonstrates that the ICs and the PCs can interrupt the crack infilling process and lead to a premature state of crack saturation compared with the concept model.

4.2 Influence of thickness of substrate layer

In this section, the influence of thickness of substrate layer on S_s/T_f is investigated. Two series of numerical results are illustrated in Fig. 16, one for shear strength of 7.2 MPa and the other for shear strength of 16.0 MPa. For each series, the thickness of the substrate layer ranges from 5 mm to 100 mm. The results indicate that the thickness of the substrate layer has negligible effect on the crack spacing to layer thickness ratio at crack saturation, S_s/T_f.

4.3 Influence of strength of top layer

Fig. 17 shows the influences of compressive strength of the top layer on τ_{cr}. The compressive strength of the top layer ranges from 20 MPa to 250 MPa. For each model with varied compressive strength, the interfacial shear strength is adjusted to obtain the τ_{cr} and S_s/T_f. The results indicate that τ_{cr} increases with increasing the compressive strength of the top layer. And S_s/T_f also increases as increasing the compressive strength.

4.4 Influence of overburden pressure (P)

In this section, various values for P are adopted to influences of overburden pressure on the threshold for shear strength while other parameters are unchanged. The result indicates that the value of P has no obvious influences on the threshold for shear strength as P increases from 0.0MPa to 8 MPa. If P ranges from 0.0 MPa to 2 MPa, S_s/T_f is almost at the same level. However, if P exceeds 2MPa, S_s/T_f decreases as P increases.

5. Conclusions

Crack behaviour of top layer in layered rocks is discussed based on a two-layer system in this study. The following conclusions could be suggested. The interface delamination and interface debonding are quite different. The interface delamination always occurs if the interface shear strength is lower. The formation of the interface delamination can reduce the load from the adjacent layers and thus prevent or delay the further infilling of vertical cracks. The interface-parallel cracking occurs at a higher interface shear strength. As a result, the interface delamination produces wider crack spacing because it happens earlier than layer-parallel fracturing. This may provide a method to discriminate interface delamination from interface-parallel cracking. It should be noted that the interface-parallel cracks obtained in this numerical simulation need to be further validated in the fields.

(1) The stress state in a crack-bound block can change from tensile to compressive as the crack spacing to layer thickness ratio decreases to a certain value. The stress state transition excludes the further infilling of the VCs in the top layer of the two-layer system.

(2) The crack patterns of the two-layer rock system are controlled by the threshold for interfacial shear strength. If the shear strength is lower than the threshold, the top layer is cracked by the VCs combing with the ICs. If the shear strength is lower than the threshold, the top layer is cracked by the VCs and PCs. If the shear strength is close to the threshold for shear strength, a combining pattern of VCs, PCs and ICs can be formed.

(3) The shear strength has a dominating influence on the ratio of crack spacing to layer thickness at crack saturation if the shear strength is lower than its threshold. For case of the shear strength greater than its threshold, it has no effect on the crack spacing to layer thickness ratio at crack saturation. The ICs and the PCs can reduce the stress transferred from the substrate layer of the two-layer system and thus lead to an immature state of crack saturation.

(4) The threshold for shear strength and ratio of crack spacing to layer thickness at crack saturation have a close relationship with the strength of the top layer that both increase as increasing the strength of top layer. The thickness of the substrate layer has little effect on crack behaviours of the top layer. The overburden pressure has no obvious influence on threshold for shear strength while it can decrease the crack spacing to thickness ratio during the infilling process.

Acknowledgements

The work described in this paper was fully supported by National Natural Science Fund of China (No. 51304067, 41172244), the National Basic Research Program of China (973 Programs: No. 2014CB047100), the Distinguished Young Scholars of Henan Polytechnic University (No. J2015-1) and the Fundamental Research Funds for the Universities of Henan Province (No. NSFRF140206).

References

Arora, S. and Mishra, B. (2015), “Investigation of the failure mode

of shale rocks in biaxial and triaxial compression tests", *J. Rock Mech. Min. Sci.*, **79**, 109-123.
Aydan, Ö., Akagi, T. and Kawamoto, T. (1993), "The squeezing potential of rocks around tunnels theory and prediction", *Rock Mech. Rock Eng.*, **26**(2), 137-163.
Bai, T., Pollard, D.D. and Gao, H. (2000), "Explanation for crack spacing in layered materials", *Nature*, **403**(6771), 753-756.
Bejari, H. and Hamidi, J.K. (2013), "Simultaneous effects of joint spacing and orientation on TBM cutting efficiency in jointed rock masses", *Rock Mech. Rock Eng.*, **46**(4), 897-907.
Ben-Zion, Y. and Lyakhovsky, V. (2002), *Accelerated Seismic Release and Related Aspects of Seismicity Patterns on Earthquake Faults*, in *Earthquake Processes: Physical Modelling, Numerical Simulation and Data Analysis Part II*, Birkhäuser, Basel, Switzerland.
Chang, X., Shan, Y.F., Zhang, Z.H., Tang, C.A. and Ru, Z.L. (2015), "Behavior of propagating fracture at bedding interface in layered rocks", *Eng. Geol.*, **197**, 33-41
Dugdale, D. (1960), "Yielding of steel sheets containing slits", *J. Mech. Phys. Solids*, **8**(2), 100-104.
Engelder, T., Lash, G.G. and Uzcátegui, R.S. (2009), "Joint sets that enhance production from Middle and Upper Devonian gas shales of the Appalachian Basin", *AAPG Bull.*, **93**(7), 857-889.
Ferrill, D.A., Morris, A.P. and McGinnis, R.N. (2012), "Extensional fault-propagation folding in mechanically layered rocks: The case against the frictional drag mechanism", *Tectonophysics*, **576**, 78-85.
Gross, M.R. and Engelder, T. (1995), "Crack strain in adjacent units of the Monterey Formation: Scale effects and evidence for uniform displacement boundary conditions", *J. Struct. Geol.*, **17**, 1303-1318.
Guo, L., Latham, J.P. and Xiang, J. (2017), "A numerical study of fracture spacing and through-going fracture formation in layered rocks", *J. Solid Strut.*, **110**, 44-57.
Jesus, A.P., Mateus, A., Munha, J.M., Tassinari, C.C.G., Santos, T.M.B. and Benoif, M. (2016), "Evidence for under plating in the genesis of the Variscan Synorogenic Beja Layered Gabbroic Sequence and related mesocratic rocks", *Tectonophyics*, **683**, 148-171.
Li, Z., Li, L., Li, M., Zhang, L., Zhang, Z., Huang, B. and Tang, C.A. (2017), "A numerical investigation on the effects of rock brittleness on the hydraulic fractures in the shale reservoir", *J. Nat. Gas Sci. Eng.*, **50**, 22-32
Lyakhovsky, V., Ben-Zion, Y. and Agnon, A. (1997), "Distributed damage, faulting, and friction", *J. Geophys. Res.*, **102**(B12), 27635-27649.
Shor, O. and Vaziri, R. (2017), "Application of the local cohesive zone method to numerical simulation of composite structures under impact loading", *J. Imp. Eng.*, **104**, 127-149.
Tabiei, A. and Zhang, W. (2017), "Cohesive element approach for dynamic crack propagation: Artificial compliance and mesh dependency", *Eng. Fract. Mech.*, **180**, 23-42.
Tang, C.A., Liang, Z.Z., Zhang, Y.B., Chang, X., Tao, X., Wang, D.G., Zhang, J.X., Liu, J.S., Zhu, W.C. and Elsworth, D. (2008), "Crack spacing in layered materials: A new explanation based on two-dimensional failure process modeling", *Am. J. Sci.*, **308**(1), 49-72.